SAIC-00/8007:APPAT-241
March 22, 2000

THE STRUCTURE AND DYNAMICS OF THE SOLAR CORONA AND INNER HELIOSPHERE

NASA SPACE PHYSICS THEORY CONTRACT NAS5-99188

SECOND Quarter FIRST YEAR PROGRESS REPORT

Covering the period November 16, 1999 to February 15, 2000

Science Applications International Corporation

An Employee-Owned Company

Submitted by:

ZORAN MIKIC

PRINCIPAL INVESTIGATOR:

SCIENCE APPLICATIONS INTERNATIONAL CORPORATION

10260 CAMPUS POINT DRIVE

SAN DIEGO, CA 92121-1578

MARCH 22, 2000

SECOND QUARTER FIRST YEAR PROGRESS REPORT

This report covers technical progress during the second quarter of the first year of NASA Sun-Earth Connections Theory Program (SECTP) contract "The Structure and Dynamics of the Solar Corona and Inner Heliosphere," NAS5-99188, between NASA and Science Applications International Corporation, and covers the period November 16, 1999 to February 15, 2000. Under this contract SAIC and the University of California, Irvine (UCI) have conducted research into theoretical modeling of active regions, the solar corona, and the inner heliosphere, using the MHD model.

In the following sections we summarize our progress during this reporting period. Full descriptions of our work can be found in the cited publications, a few of which are attached to this report.

The Initiation of Coronal Mass Ejections by Emerging Flux

Eruptive solar phenomena, such as coronal mass ejections, are believed to be initiated by the release of energy stored in the coronal magnetic field. Nonpotential magnetic field structures with significant amounts of free magnetic energy are known to exist in the corona. However, the mechanism by which this energy is released are not well understood. Observations of disappearing filaments imply that coronal mass ejections (CMEs) might be triggered by newly emerging magnetic field in the neighborhood of a streamer (Feynman & Martin 1995). We have studied theoretically the effect of emerging flux on the stability of helmet streamers. We have found that the emergence of new magnetic flux can lead to disruption of a helmet streamer, with liberation of a significant fraction of the stored magnetic energy. One way that this can occur is when magnetic flux of opposite polarity emerges in the vicinity of the neutral line, canceling some of the ambient flux. When the amount of emerged flux is below a threshold, a stable streamer equilibrium with a flux rope results. When the threshold is exceeded, the streamer erupts and leaves the Sun with a substantial amount of kinetic energy. Both 2D (axisymmetric) and 3D simulations illustrating this process have been completed. A paper that explores the eruption of arcades has been published in the *Astrophysical Journal* (Amari *et al.* 2000), and is included in the Appendix.

Modeling the Magnetic and Thermal Structure of Coronal Loops and Prominences

We have used our 3D MHD code in Cartesian coordinates to study the magnetic structure of solar prominences. Our model has been motivated by observations of a quiescent prominence on September 23, 1996. To form the magnetic field required to support a prominence, we started with a potential magnetic field with a flux distribution similar to that observed. We applied shear flows near the neutral line to generate a non-potential magnetic field. We then canceled magnetic flux in order to form a magnetic field that had a flux-rope topology that could support a prominence. We will continue to study the magnetic field topology of the prominence by adding parasitic polarities in the vicinity of the neutral line in an effort to produce the "barbs" that are seen in Hα images of the prominence.

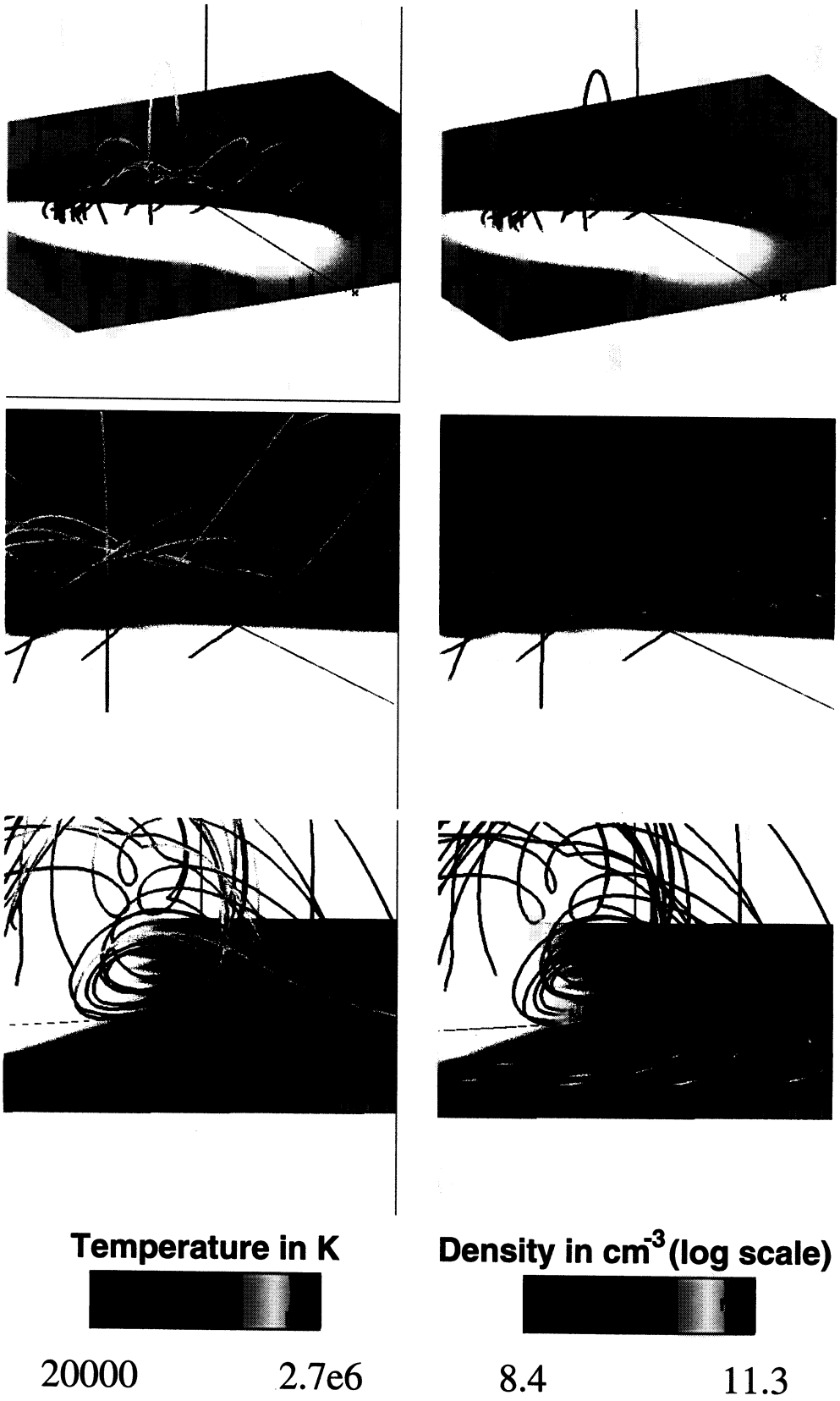

Figure 1. Three different views of field lines in a model of the magnetic field in a prominence. The flux rope that lies along the neutral line can support cool, dense material. The left panels show field lines colored by the temperature along the field line, while the right panels show field lines colored by the density. Notice that the cool, dense material sits at the bottom of the dips of the field lines in the flux rope.

We have also performed 1D hydrodynamic solutions along field lines extracted from the 3D MHD simulations, with an energy equation that includes thermal conduction, heating and radiation losses. We have shown that condensations are formed in the dips of the field lines belonging to the flux rope (see Figure 1). This work implies that magnetic flux ropes along neutral lines can provide the support for the cool and dense material of prominences. These results were presented at the Fall Meeting of the American Geophysical Union, held in San Francisco, Dec. 13–17, 1999, in the paper "Magnetic Field Topology and Modeling of Loops in Prominences," by R. Lionello, Z. Mikić, and J. A. Linker. A manuscript reporting on this work is in preparation (Lionello, Mikić, & Linker 2000).

The Heliospheric Current Sheet at Various Phases of the Solar Cycle

We have developed a three-dimensional MHD model to investigate the large-scale structure of the heliosphere (out to 5 AU) at various epochs of the solar cycle. We use the magnetic field topology from a coronal solution to generate flow fields at the inner boundary of the heliospheric model (30 solar radii), which is in turn driven by observations of the line-of-sight component of the photospheric magnetic field. In Figure 2, we use results from the heliospheric model to illustrate the evolution of the Heliospheric Current Sheet (HCS) over the course of a solar cycle. The first panel shows the HCS near solar minimum. The single fold in the surface maps back to ~ 180–270 degrees longitude, and can be correlated with a northward extension of the slow flow band at the Sun. Note that this fold is radially asymmetric, with its outer edge being sharper than its inner edge. This results from fast solar wind at ~ 280 degrees overtaking slower wind ahead accelerating it and steepening the HCS profile. Conversely, at the inner edge of the deformation , the HCS is "stretched out" as faster wind outruns slower wind creating a rarefaction region, or expansion wave. This picture differs from ones produced by kinematic models of the HCS, which assume that the speed of the plasma remains constant as the plasma moves out from the Sun. In the middle panel, the HCS during the time of Ulysses' "rapid latitude scan" is shown. Now, two folds dominate the HCS profile and are in qualitative agreement with the sector structure observed by Ulysses during this time period. Finally, the HCS for Carrington rotation 1947 is shown in the bottom panel. The HCS is again dominated by two folds that extend up to ~ 40–55 degrees. In contrast to solar minimum, however, the folds are more symmetric, since the wind surrounding them does not have the same large variations in speed. A manuscript based on this work is in preparation (Riley, Linker, & Mikić 2000). This work was presented at the Fall AGU Meeting in held in San Francisco, Dec. 13–17, 1999 (with J. Gosling).

MHD Modeling of the Solar Corona: Solar Minimum and Solar Maximum

In the past few years our three-dimensional magnetohydrodynamic (MHD) models of the solar corona have advanced to the point that computations for specific time periods can be performed and compared with observations. With the rise of the solar cycle, we have now performed computations for recent time periods when the sun is near its most active phase. We are thus able to compare and contrast the properties of the solar minimum and maximum

Heliospheric Current Sheet at 3 Epochs of the Solar Cycle

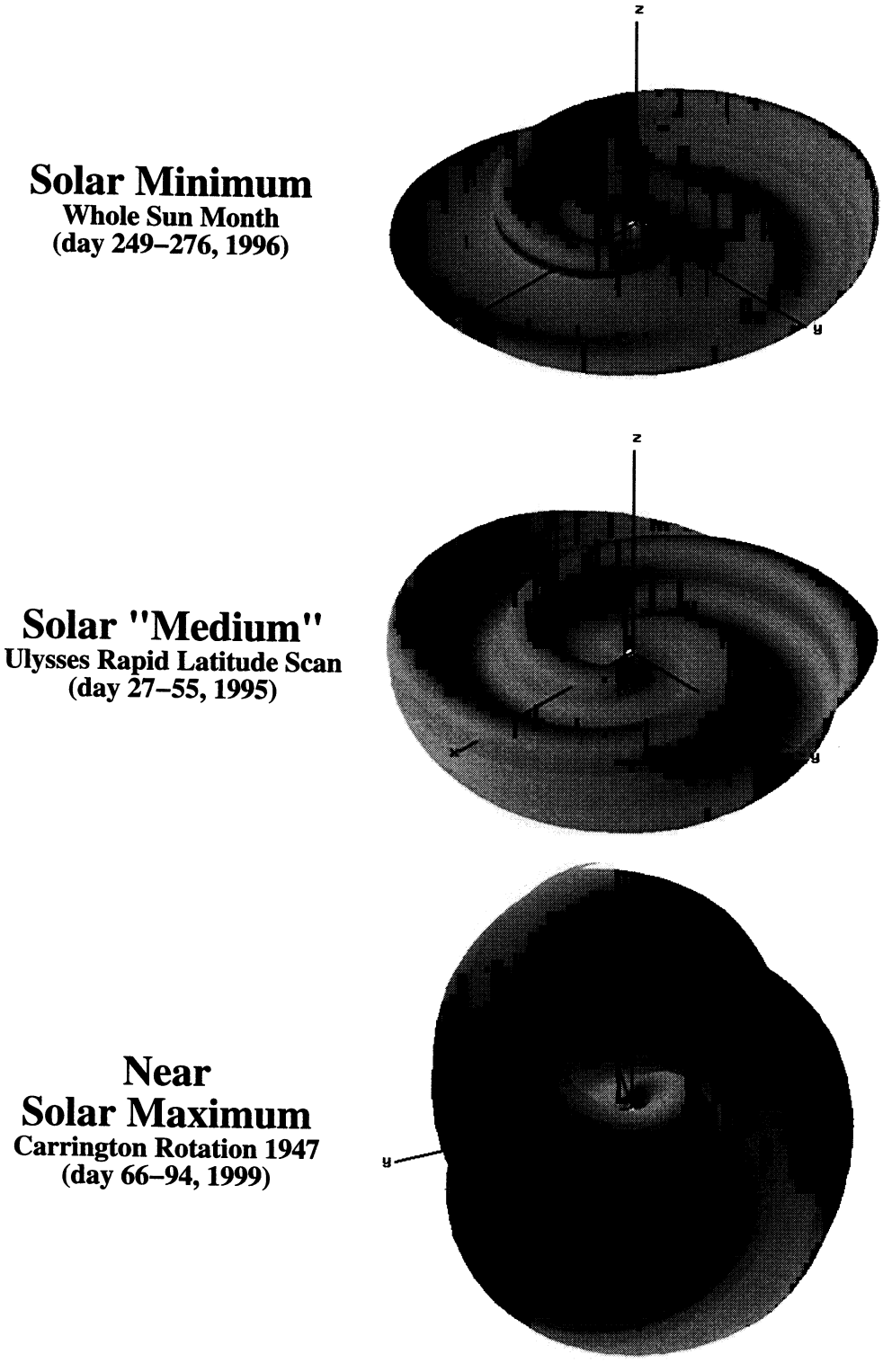

Figure 2. The heliospheric current sheet (HCS) at three different times of the solar cycle, as computed from 3D MHD simulations.

corona. In Figure 3 we compare the polarization brightness (pB) from our MHD simulation of Carrington rotation 1951 (June 24–July 21, 1999) with coronagraph observations from the Mauna Loa MK3 instrument. This material was presented in an invited talk, "Magnetohydrodynamic Modeling of the Solar Corona: Solar Minimum and Solar Maximum," by J. Linker and Z Mikić at the Fall AGU Meeting, held in San Francisco, Dec. 13–17, 1999,

The Structure of the Sun During Low-Density Solar Wind Periods

In a collaboration we studied the three-dimensional Sun for the dates surrounding the period of extremely low density solar wind on May 10–12, 1999, along with several other intervals of low solar wind density. Representations of the source of the solar wind include synoptic data of the surface magnetic fields, and He I 10830, EUV coronal and white light coronagraph images. The solar wind data include temperature, density, composition and magnetic field data from the SOHO, ACE and WIND spacecraft. Two models were examined to provide possible interpretations: source-surface magnetic field maps and a 3-D MHD simulations. The paper "The Structure of the Sun During Low-Density Solar Wind Periods," by B. J. Thompson, D. A. Biesecker, K. L. Harvey, T. Hoeksema, J. A. Linker, Z. Mikić, H. R. Norton, K. W. Ogilvie, A. Posner, P. Riley, & T. Zurbuchen, was presented at the Fall AGU Meeting, held in San Francisco, Dec. 13–17, 1999.

The Use of Composition Data to Study the Origin of Open Magnetic Field Lines

Recently, Fisk *et al.* (1999) presented a theory that describes a number of features of the large-scale coronal and heliospheric magnetic field. This theory predicts large-scale transport of magnetic flux, which leads to reconnection processes at low latitudes. The reconnection process reveals itself in solar wind composition data: plasma released out of previously closed magnetic field structures exhibits hotter charge state distributions and has a tendency to be enriched by elements with low first ionization potentials. In a collaboration, we used Ulysses-SWICS composition measurements and numerical models (Linker *et al.* 1999; Riley *et al.* 1999) to accurately map these observations back to the solar surface. We compared the locations of these source regions with SOHO observations of the low corona. The results were interpreted in the context of the global structure of the heliospheric magnetic field. The paper "The Origin of Open Magnetic Field-Lines at the Sun Revealed by Composition Data and Numerical Models," by A. Posner, T. H. Zurbuchen, N. A. Schwadron, L. A. Fisk, G. Gloeckler, J. A. Linker, Z. Mikić, & P. Riley, was presented at the Fall AGU Meeting, held in San Francisco, Dec. 13–17, 1999,

Modeling the Corona and Inner Heliosphere During "Whole Sun Month 3"

In January 2000, Zoran Mikić, Jon Linker, and Pete Riley attended the "Whole Sun Month 3" Workshop. This is a follow-on to the very successful "Whole Sun Month" (WSM) workshop that examined the Sun during a time of solar minimum in August–September, 1996. As a result of collaborations fostered by the first workshop, a special issue of

Comparison of an MHD Model with MK3 Coronameter Images near Solar Maximum

Carrington Rotation 1951: June 24 – July 21, 1999

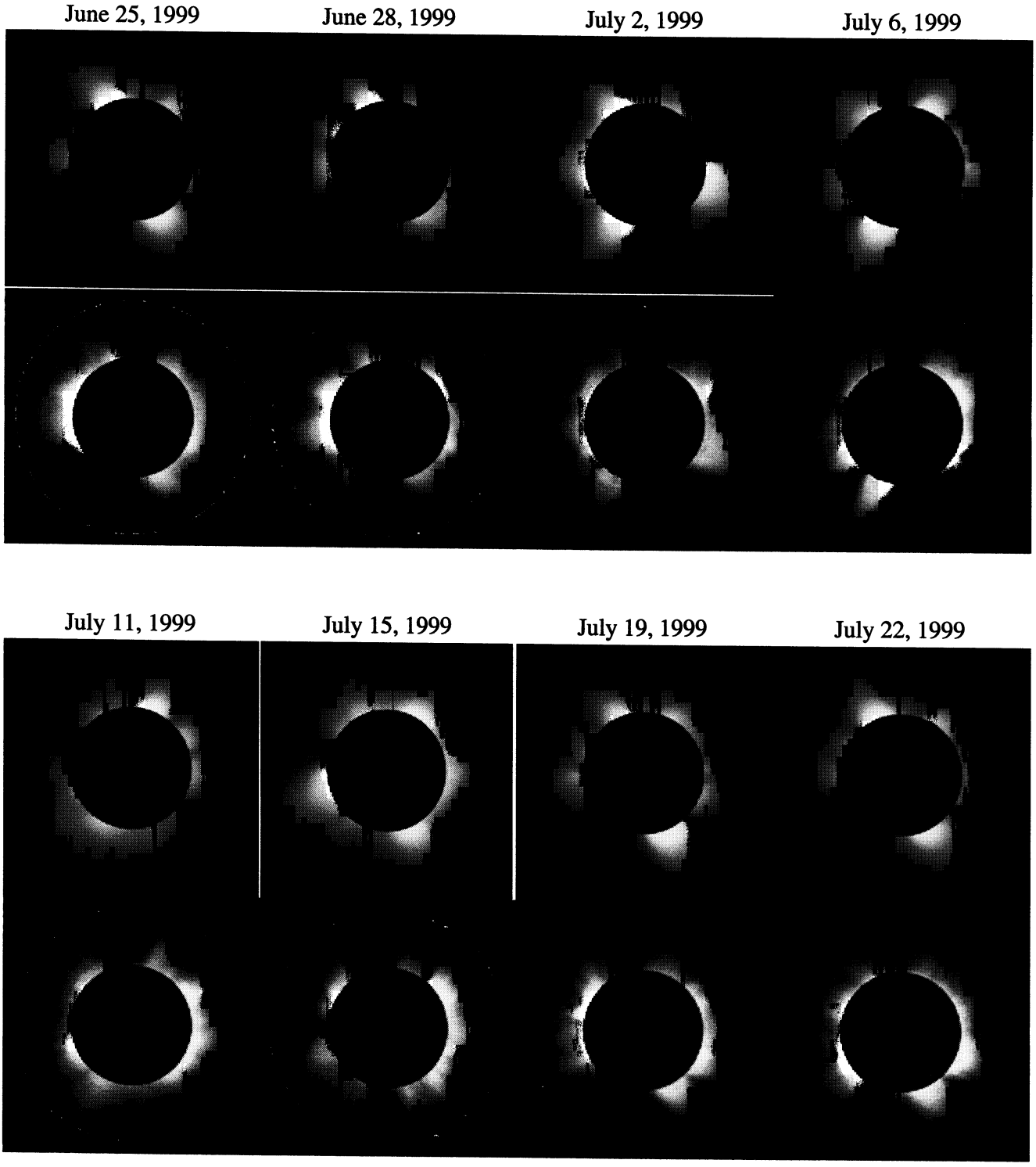

Figure 3. Comparison of the polarization brightness (pB) observed with the Mauna Loa MK3 coronagraph and that computed from a 3D MHD simulation. The panels compare the observations and the model during one solar rotation (Carrington rotation 1951; June–July 1999).

the *Journal of Geosphysical Research* was published in May 1999. The WSM3 workshop will look at the Sun during Carrington rotation 1953 (Aug. 18–Sep. 14, 1999), a time when the Sun is approaching solar maximum, with a considerable increase in complexity compared to the WSM period. We will apply our 3D MHD model to modeling the corona and solar wind during this time interval.

Progress in Parallelizing the MAS Code

Comparison with the NIMROD Code

A comparative test of the parallel efficiency has been performed between the parallel MAS code and the NIMROD code. Like MAS, NIMROD solves 3D MHD nonlinear problems with a pseudospectral method, although it does not have a staggered mesh for the field variables. NIMROD is used in fusion research and has been designed as a parallel code from the very beginning. Both codes behave similarly when the grid size on each processor is large. This gives us confidence that the parallelization of the MAS code is being done in a reasonable way. The parallel efficiency is greater than 80% for a 2×2 processor decomposition. The parallel efficiency decreases when the number of grid points per processor becomes too small.

Advanced Parallel I/O

The most common way of performing parallel I/O is through a proper gather/scatter of data between all the processors, with one processor selected as the front-end for writing to/reading from disk files. For large problems this approach may not be viable, since it requires the creation in memory of an array large enough to store the global mesh. On large problems this may require more memory than is available.

To overcome this problem the I/O algorithm has been modified so that each processor writes out (reads in) its portion of the global array from (to) different locations of the same direct access file. This algorithm allows us to have the same structure of the restart file independently of the number of processor used to decompose the problem, increasing the flexibility of the resulting code. An alternative scheme, using (faster) sequential access files, but with a more complex indexing and synchronization algorithm, is presently under investigation.

Porting the MAS Code to Different Parallel Architectures

The parallel MAS code has been primarily developed and tested on the Cray T3E supercomputer. The latest version of the code has been made completely platform independent, using Fortran 90, and has been compiled on other parallel machines, including HP Exemplar, SGI Origin, IBM SP3, and SGI R12000 multiprocessors. Optimization and testing on these machines is currently under way.

REFERENCES

Amari, T., Luciani, J.-F., Mikić, Z., & Linker, J. A. 2000, *Ap. J.*, **529**, L49.

Feynman, J., & Martin, S. F. 1995, *J. Geophys. Res.*,**100**, 3355.

Fisk, L. A., Zurbuchen, T. H., & Schwadron, N. A. 1999, *Ap. J.*, **521**, 868.

Linker, J. A., Mikić, Z., Biesecker, D. A., Forsyth, R. J., Gibson, S. E., Lazarus, A. J., Lecinski, A., Riley, P., Szabo, A., & Thompson, B. J. 1999, *J. Geophys. Res.*, **104** , 9809 (1999).

Riley, P., Gosling, J. T., McComas, D. J., Pizzo, V. J., Luhmann, J. G., Biesecker, D., Forsyth, R. J., Hoeksema, J. T., Lecinski, A., & Thompson, B. J. 1999, *J. Geophys. Res.*, **104**, 9871.

APPENDIX

SELECTED REPRINTS

THE ASTROPHYSICAL JOURNAL, 529:L49–L52, 2000 January 20

A TWISTED FLUX ROPE MODEL FOR CORONAL MASS EJECTIONS AND TWO-RIBBON FLARES

T. AMARI[1]
DSM/DAPNIA, Service d'Astrophysique, URA 2052 associée au Centre National de la Recherche Sientifique, CEA-Saclay, F-91191 Gif sur Yvette Cedex, France; amari@discovery.saclay.cea.fr
J. F. LUCIANI
Centre National de la Recherche Sientifique, Centre de Physique Théorique de l'Ecole Polytechnique, F-91128 Palaiseau Cedex, France
AND
Z. MIKIC AND J. LINKER
Science Applications International Corporation, 10260 Campus Point Drive, San Diego, CA 92121
Received 1999 July 13; accepted 1999 November 29; published 1999 December 22

ABSTRACT

We present a new approach to the theory of large-scale solar eruptive phenomena such as coronal mass ejections and two-ribbon flares, in which twisted flux tubes play a crucial role. We show that it is possible to create a highly nonlinear three-dimensional force-free configuration consisting of a twisted magnetic flux rope representing the magnetic structure of a prominence (surrounded by an overlaying, almost potential, arcade) and exhibiting an S-shaped structure, as observed in soft X-ray sigmoid structures. We also show that this magnetic configuration cannot stay in equilibrium and that a considerable amount of magnetic energy is released during its disruption. Unlike most previous models, the amount of magnetic energy stored in the configuration prior to its disruption is so large that it may become comparable to the energy of the open field.

Subject headings: MHD — stars: coronae — stars: flare — stars: magnetic fields

1. INTRODUCTION

The search for various mechanisms that can trigger large-scale eruptive phenomena such as coronal mass ejections (CMEs) or two-ribbon flares has been given a great deal of attention for several decades. Most axisymmetric models have neglected the prominence prior to the CME and have considered the destabilization of an arcade (representing the overlaying structure) driven by photospheric shearing motions (in Cartesian geometry [Amari et al. 1996a] and spherical [Mikic & Linker 1994]). This important assumption implies that a passive role is played by the prominence that would be ejected as part of the structure.

Three-dimensional models have only recently started to be considered. An initially arcade-like configuration can open in finite time when photospheric twisting motions are applied to its footpoints (Amari et al. 1996b). No plasmoid or current sheet is created during the evolution. Moreover, no sufficient amount of magnetic energy has ever been released in previous three-dimensional simulations. In a recent new approach, an important role is played by twisted flux ropes. These represent an important source of magnetic helicity in the corona and may be used to model the prominence's global magnetic support (Amari et al. 1999c). They correspond to new three-dimensional solutions for the MHD equations obtained by the diffusion introduced to the boundary so as to model the dispersion of the active-region flux in the network (Wang, Sheeley, & Nash 1991).

In this Letter, we consider a new and different mechanism consisting of two phases: (1) photospheric shearing and (2) opposite-polarity emergence. In § 2, we present the different MHD phases that may lead to the generation of the twisted flux-tube solutions. In § 3, we discuss the disruption phase.

[1] Also at Centre National de la Recherche Sientifique, Observatoire de Paris, Laboratoire de Physique Solaire et de l'Heliosphere, F-92195 Meudon Principal Cedex, France.

2. FORMATION OF THE TWISTED FLUX TUBE

Let us consider at time $t = 0$ an initial current-free magnetic configuration having an arcade-like topology (Fig. 1*a*) in the upper corona that is represented by the domain $D = \{z > 0\}$ and is numerically approximated by the finite box $\{0 < x < L_x,\ 0 < y < L_y,\ 0 < z < L_z\}$ whose size $L_x = L_y = L_z = 40$–60 (in unit of the characteristic length scale of the system) is large. This initial condition is the same as in Amari et al. (1999c) and is obtained by solving the Laplace equation for the scalar potential $\Psi(x, y, z)$ associated with $\boldsymbol{B}$ for Dirichlet-Neuman boundary conditions on ∂D. On the boundary $\{z = 0\}$, these correspond to the distribution given by two elliptic Gaussian functions symmetrically placed across the x-axis. Their centers are $(0, \pm 0.8)$, their width is $(\delta x = 1,\ \delta y = 2)$, and the normalization is such that the maximum value taken for B_z is 1.

For $t \geq 0$, we generate an MHD evolution using the configuration above as an initial condition. To advance the equations, we use our MHD code METEOSOL (Amari, Luciani, & Joly 1999a), which solves the MHD equations that are exactly those given in Amari & Luciani (1999) and Amari et al. (1999c). These are discretized on a nonuniform mesh ($111 \times 101 \times 70$ nodes) with the same assumptions: $\beta = 0$, gravity is neglected, and viscosity $\nu = 10^{-2}$ to 10^{-3}. This evolution consists of the following three steps:

1. A first shearing phase from $t = 0$ to $t = 200$ (in units of the Alfvén time) generates an evolution driven by slow boundary twisting motions on $\{z = 0\}$ ($v_0 = 10^{-2}$; then v_0 is small compared with the Alfvén speed $v_A = 1$). As in Amari et al. (1996b) and Amari et al. (1999c), these consist of two parallel vortices that bring up a high shearing motion near the neutral line, while a twisting motion is introduced as one moves away from the neutral line on $\{z = 0\}$. The resistivity is fixed at $\eta = 0$ during this phase, which is found to be almost quasi-static.

2. At $t = 200$, the driving photospheric velocity field is switched off, and one lets the system evolve through a viscous

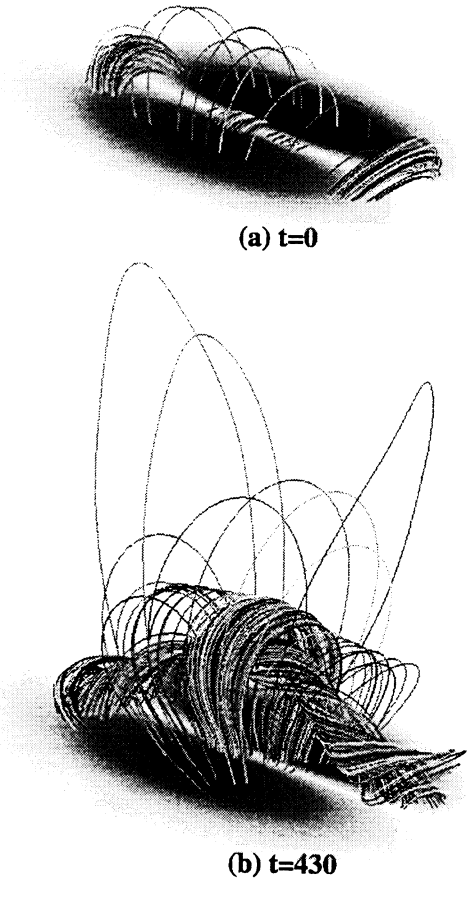

FIG. 1.—Selected field line of the configuration at two steps of the MHD evolution in units of τ_A: (*a*) $t = 0$, and (*b*) $t = 430$ when a twisted flux rope has been created.

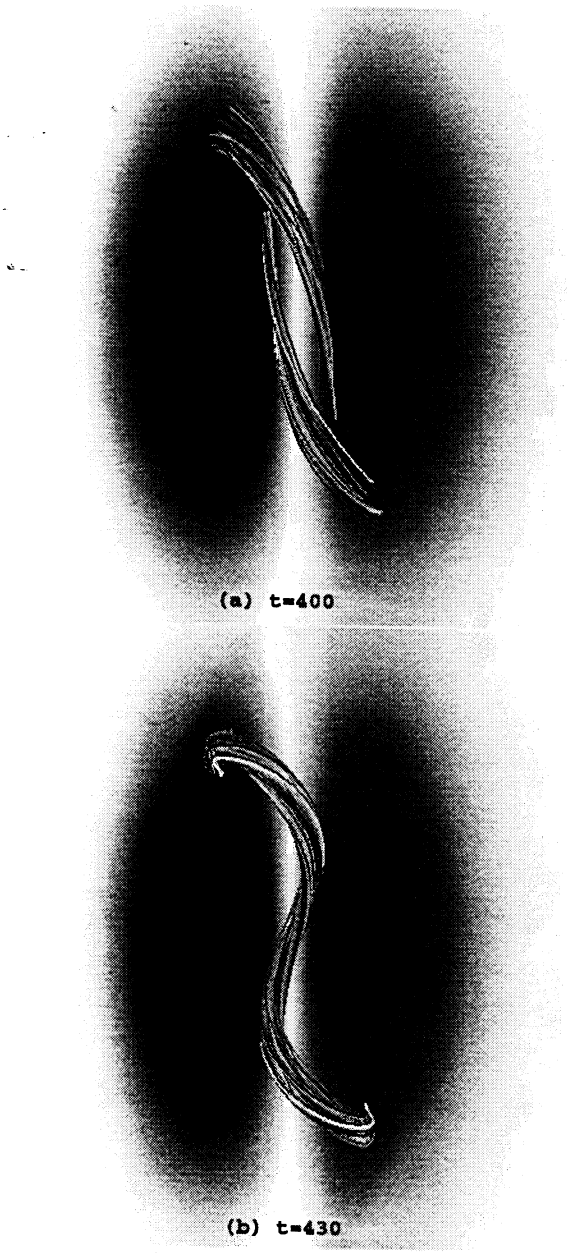

FIG. 2.—Top view of selected field lines showing the merging of two inverse J-shaped structures visible at (*a*) $t = 400$ into a single inverse S-shaped structure at (*b*) $t = 430$.

relaxation procedure that is stopped at $t = 400$ when the system has relaxed to an accessible stable numerical force-free equilibria. This one corresponds to a highly sheared magnetic configuration (an angle of about 70°–75° along the neutral line is found), which is typically observed in active regions (Heyvaerts & Hagyard 1991).

3. Then, for $t > 400$, two opposite polarities start emerging. Each one is located at the center of one spot of the configuration obtained at $t = 400$ and has the opposite sign. The boundary velocity is kept switched off all along this phase ($\boldsymbol{v}|_{\partial D} = 0$). This a different type of boundary condition than the one used in Amari et al. (1999c). We have also chosen different values for the resistivity ($\eta = 10^{-4}$ and 10^{-5}) and found similar results. Figure 1*b* shows the final stage, which is chosen to be $t = 430$ in this study.

During this third phase, a twisted magnetic flux rope aligned with the neutral line and embedded in an overlaying, almost potential, arcade is created. The presence of magnetic dips is favorable to the material support of prominence (Amari et al. 1999c). Figure 2 shows an interesting feature occurring during the last step of the evolution. As the twisted flux rope forms, two inverse J-shaped structures join to form a single inverse

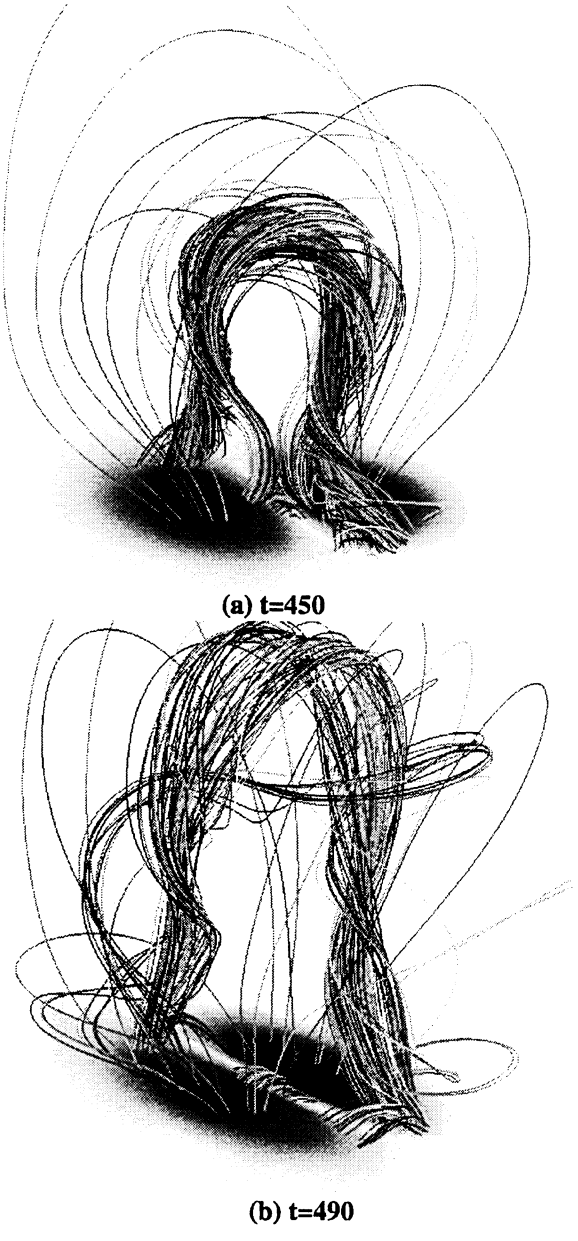

FIG. 3.—Evolution of the configuration shown on Fig. 1*b* at two steps during a relaxation phase at (*a*) $t = 450$ and (*b*) $t = 490$. No neighboring equilibria exist, and the configuration experiences a major disruption.

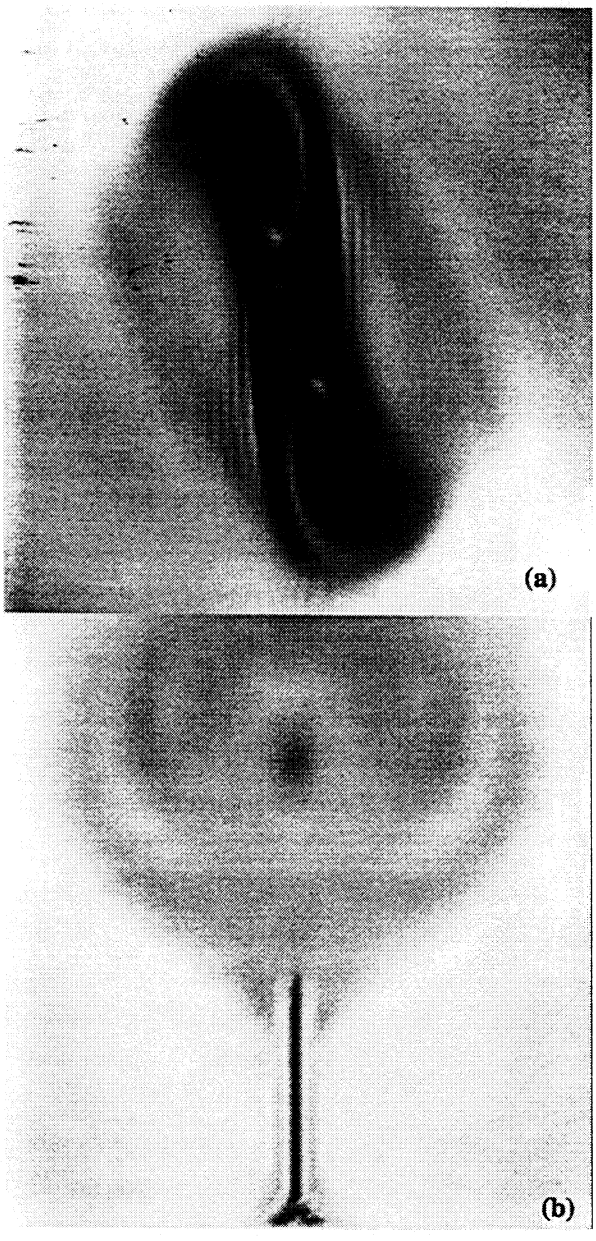

FIG. 4.—Cuts of α (the measure of electric currents) at two steps of the evolution: (*a*) the horizontal cut above the twisted flux tube at $t = 430$, also confirming the inverse S-shaped structure seen in Fig. 2*b*, and (*b*) the vertical cut in the central plane $\{x = 0\}$ during the reconnection phase at $t = 450$.

S-shaped structure. This structure is confirmed by the horizontal cut of $\alpha = \boldsymbol{J} \cdot \boldsymbol{B} / |\boldsymbol{B}|^2$ (measuring the electric currents) above the twisted flux rope (as shown on Fig. 4*a* below). This kind of feature has been observed in *Yohkoh* soft X-ray telescope data and has been associated with prominences (Petsov & Canfield 1996).

3. DISRUPTION OF THE TWISTED FLUX TUBE

We now analyze the sequence of equilibria found during the third step described in § 2. One selects as an initial state of a new phase one of the states obtained at $t = t_1$, with $t_1 \in [400, 430]$. In order to test the possibility of finding an accessible neighboring equilibrium, one then applies a viscous relaxation procedure as in step 2 of § 2 for $t > t_1$. We found that the intermediate state $t_1 = 410$ reaches a neighboring equilibria (not shown here), while for $t_1 = 430$, the configuration experiences a major global disruption. The twisted flux rope expands very rapidly, as shown in Figures 3*a* and 3*b*, at two particular stages of its evolution.

As shown in Figure 3*a* (at $t = 450$), the magnetic topology of the configuration reveals several interesting features gathered

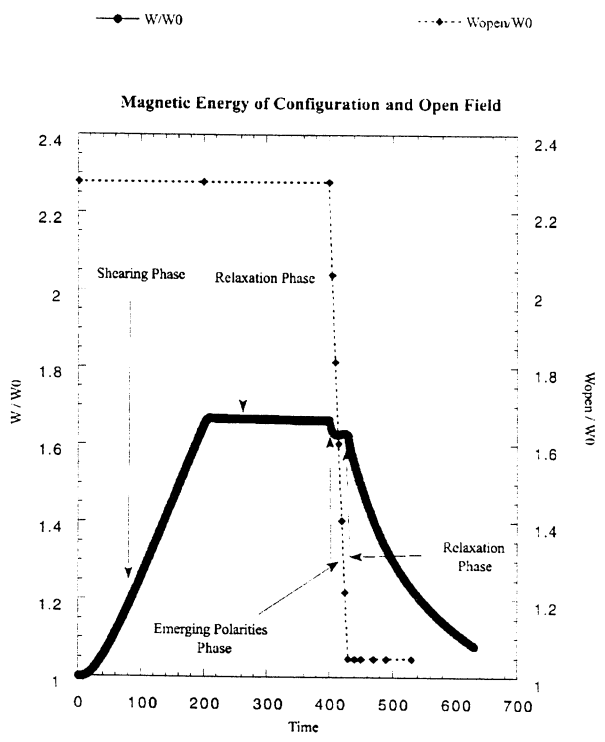

FIG. 5.—Evolution of the relative magnetic energies W/W_0 and W_{open}/W_0, where W_0 is the energy of the potential field with the same photospheric distribution for B_z. Time is in units of Alfvén time τ_A.

in a typical four-component structure: (1) the rising twisted flux rope, (2) the set of field lines that form an island through which runs the twisted flux rope, closing down below with (3) field lines defining a vertical finite-size reconnecting region, and finally (4) a set of arcades close to the boundary that reform as the reconnection goes on (and that may represent postflare loops in this model). These features are confirmed by Figure 4*b*, which shows a cut of α in the central vertical plane $\{x = 0\}$. Reconnection occurs (to our numerical resolution) through a vertical current sheet (whose existence as a true singularity of the ideal MHD equations is beyond the scope of this Letter; Amari 1991). Unlike in the axisymmetric studies, in the present three-dimensional model, the twisted flux rope is an essential ingredient at the origin of the disruption.

The evolution of the relative magnetic energy is shown in Figure 5. The new important feature is that during the phase of opposite-polarity emergence, W/W_0 decreases by only a small amount, while W_{open}/W_0 has decreased by a much larger amount, thus approaching W/W_0 from above. The consequence is that these two energies become equal at some time. In previous three-dimensional studies, attempts to increase W/W_0 so as to approach W_{open}/W_0 (from below) were all performed by applying photospheric boundary motions that increase W/W_0 monotonically as in Aly (1991). The small amount of magnetic energy dissipated during the emerging phase is due to the presence of a small but finite value of the resistivity. This third phase is associated with a change of topology (from arcade-like to flux ropelike). Furthermore, the amount of magnetic energy dissipated during the last dynamic reconnection phase is larger than that ever found by any other mechanism driven by photospheric boundary motions. In the case of a confined disruption (Amari & Luciani 1999), 5% of W_0 were released (or 30% of the energy accumulated during the twisting phase). In this new model, 55% of W_0 (or 91% of the energy accumulated during the shearing plus emerging flux phase) is released.

Our results (see, in particular, Figs. 2 and 4*b*) are in agreement with the recent studies of Canfield, Hudson, & McKenzie (1999), which show that 68% of the active regions presenting inverse S-shaped structures seen in soft X-rays lead to CMEs. We do not claim that the twisted flux rope (the prominence) is necessarily created by this process. It worth noting that Antiochos, Devore, & Klimchuck (1999) proposed a different mechanism for the complex topology configurations.

We wish to thank NATO and the Centre National d'Etudes Spatiales for their financial support. The numerical simulations performed in this Letter have been done on the CRAY supercomputers of the Commissariat à l'Energie Atomique and the Institute de Developement et des Ressources en Informatique Scientifique of the Centre National de la Recherche Scientifique.

REFERENCES

Aly, J. J. 1991, ApJ, 375, L61
Amari, T. 1991, in Advances in Solar System Magnetohydrodynamics, ed. E. R. Priest & A. W. Hood (Cambridge: Cambridge Univ. Press), 173
Amari, T., & Luciani, J. F. 1999, ApJ, 515, L81
Amari, T., Luciani, J. F., Aly, J. J., & Tagger, M. 1996a, A&A, 306, 913
———. 1996b, ApJ, 466, L39
Amari, T., Luciani, J. F., & Joly, P. 1999a, SIAM J. Sci. Stat. Comput., in press
Amari, T., Luciani, J. F., & Mikic, Z. 1999b, Plasma Phys. Controlled Fusion, 41, A779
Amari, T., Luciani, J. F., Mikic, Z., & Linker, J. 1999c, ApJ, 518, L57
Antiochos, S. K., Devore, C. R., & Klimchuk, J. A. 1999, ApJ, 510, 485
Canfield, R. C., Hudson, H. S., & McKenzie, D. E. 1999, Geophys. Res. Lett., 26, 627
Heyvaerts, J., & Hagyard, M. J. 1991, in Proc. Flares 22 Workshop, Dynamics of Solar Flares, ed. B. Schmieder & E. R. Priest (Paris: Obs. Paris), 1
Mikic, Z., & Linker, J. A. 1994, ApJ, 430, 898
Petsov, A. A., & Canfield, R. C. 1996, ApJ, 473, 533
Wang, Y. M., Sheeley, N. R., & Nash, A. G. 1991, ApJ, 383, 431

MAGNETIC FIELD TOPOLOGY AND MODELING OF LOOPS IN PROMINENCES

Roberto Lionello, Zoran Mikić,

Tahar Amari, Jon A. Linker

CES
Center for Energy and Space Science
San Diego, CA

SAIC® Science Applications International Corporation
An Employee-Owned Company

Centre de physique théorique
ECOLE POLYTECHNIQUE

Introduction

- Past research has looked for magnetic configuration to support a prominence.
- A flux rope is a viable candidate to support the dense and cooler prominence material
- It has many theoretical and observational requirements such as twist, shear along the neutral line, and dips.
- Amari *et al.* (Ap.J., **518**, L57, 1999) have shown how flux dispersal and cancellation in an idealized sheared arcade can lead to the formation of a stable flux rope structure.

- We show how the same process leads to the formation of a stable flux rope (corresponding to a prominence observed on September 23, 1996).

- The final configuration consists of a twisted magnetic flux tube embedded in an overlying, almost potential, arcade.

- Solutions of the 1D hydrodynamic equations along field lines in this configuration show that the flux rope can support cold and dense material that is characteristic of a prominence

Sacramento Peak H-α Image

Sept. 23, 1996

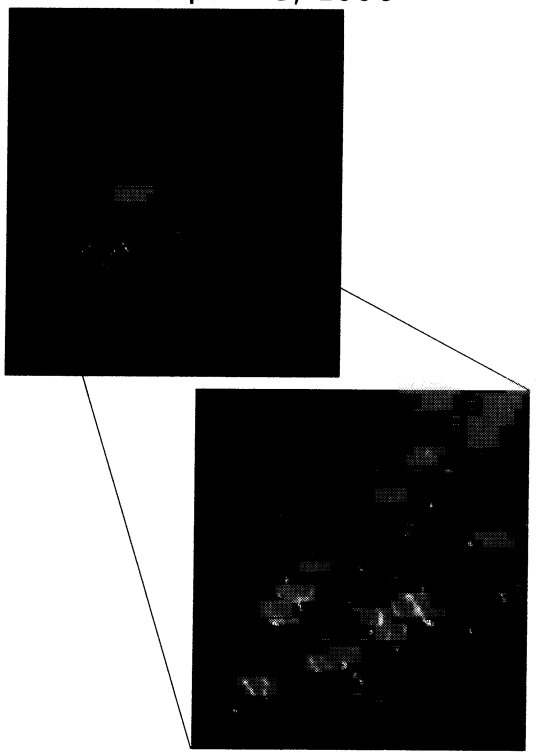

Kitt Peak Magnetogram

Sept. 23, 1996

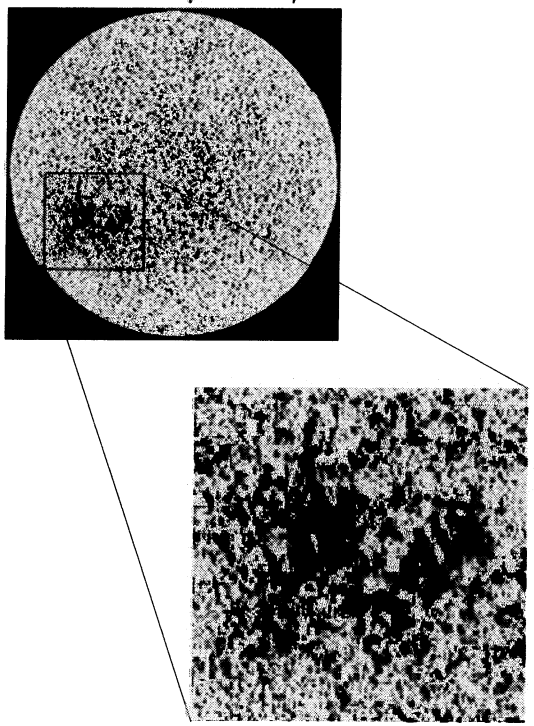

The MHD Model

$$\begin{aligned} \mathbf{E} + \frac{\mathbf{v} \times \mathbf{B}}{c} &= \eta \mathbf{J}, \\ \rho \left(\frac{\partial \mathbf{v}}{\partial t} + \mathbf{v} \cdot \nabla \mathbf{v} \right) &= \frac{1}{c} \mathbf{J} \times \mathbf{B} \\ &\quad + \nabla \cdot (\nu \rho \nabla \mathbf{v}). \end{aligned}$$

$\rho = \rho_0$ Constant density

$L \simeq 1.5 \times 10^5$ Km Active region length scale

$\tau_\nu / \tau_A = 200$ (Viscous time)/(Alfvén time)

$S = 1 \times 10^5$ Lundquist number

$51 \times 51 \times 61$ Grid.

The Simulation

- Phase 1: We find the potential field corresponding to a realistic magnetic flux distribution at the base.
- Phase 2: We apply a velocity shear localized along the neutral line.
- Phase 3: We emerge magnetic flux with opposite polarity. A flux rope is formed along the neutral line, surrounded by an arcade.

Phase 1: Potential Field

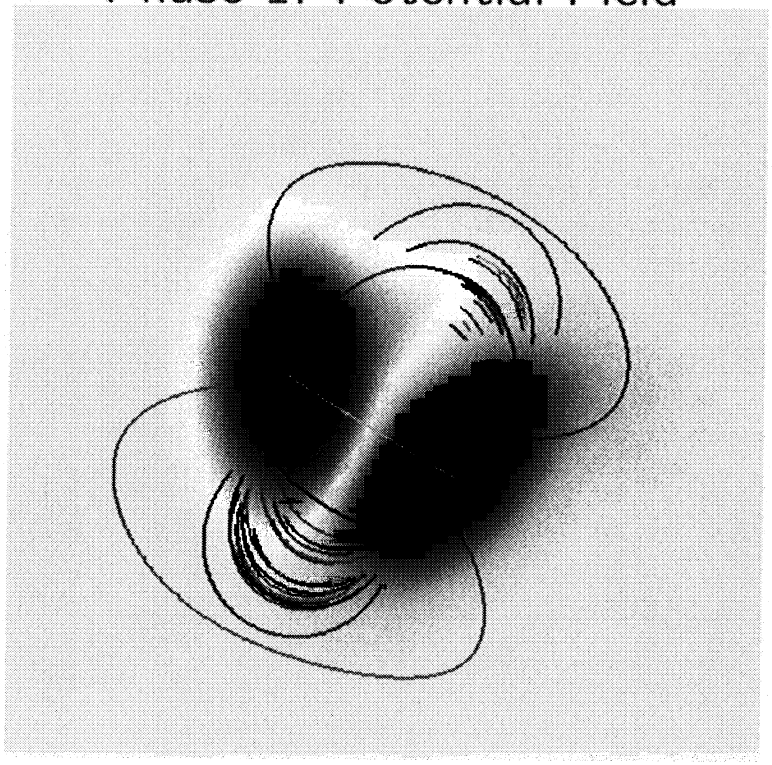

Phase 2: Shearing Phase

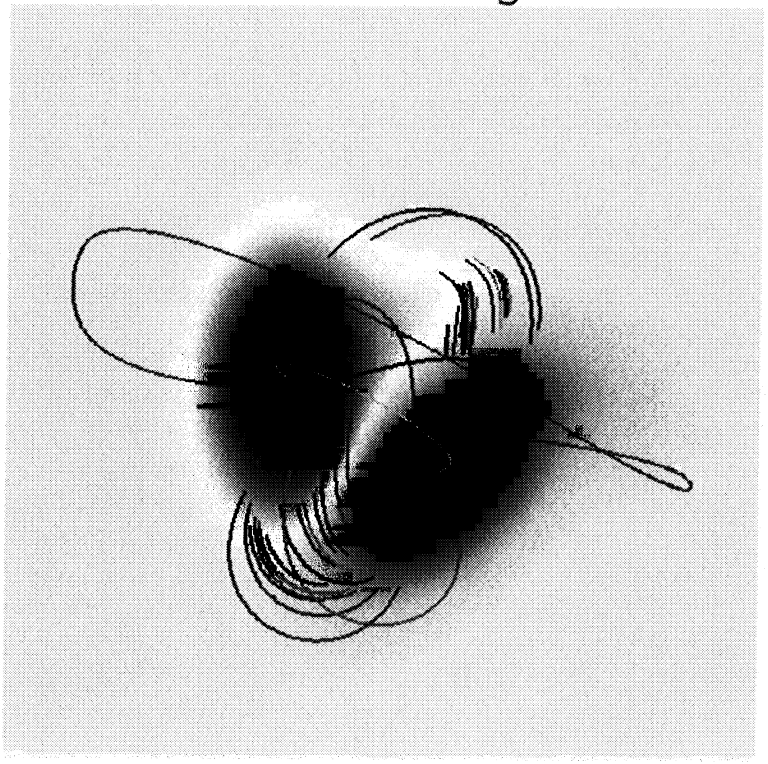

Phase 3: Flux Emergence

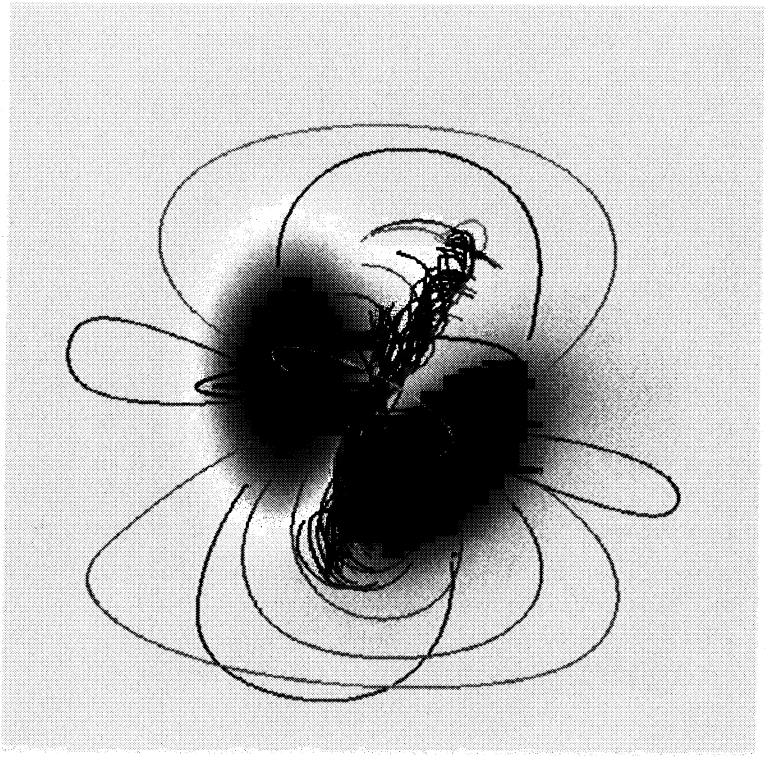

HD Solutions along Field Lines

- We solve the 1D hydrodynamic equations along several field lines.

$$\begin{aligned}
\frac{\partial \rho}{\partial t} + v\frac{\partial \rho}{\partial s} &= -\rho\frac{1}{A}\frac{\partial}{\partial s}Av, \\
\frac{\partial T}{\partial t} + v\frac{\partial T}{\partial s} &= -(\gamma-1)T\frac{1}{A}\frac{\partial}{\partial s}Av \\
&\quad -(\gamma-1)\frac{m}{k\rho}\left(\frac{1}{A}\frac{\partial}{\partial s}A\kappa T^{5/2}\frac{\partial T}{\partial s}\right. \\
&\quad \left. +n_e n_p Q(T) - H\right), \\
\rho\frac{\partial v}{\partial t} + v\frac{\partial v}{\partial s} &= -\frac{\partial p}{\partial s} - \rho g_s + \frac{1}{A}\frac{\partial}{\partial s}A\left(\nu\rho\frac{\partial v}{\partial s}\right).
\end{aligned}$$

- Heating function corresponds to an energy flux at the base of 10^6 erg cm^{-2} s^{-1} and length scale of 0.05 $R_\odot$.

- Stable condensations are formed in lines which belong to the flux rope and have dips.

Field Line without Condensation

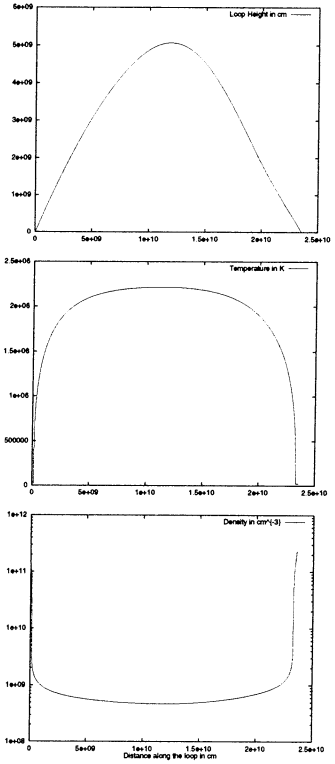

Field Line with Condensation

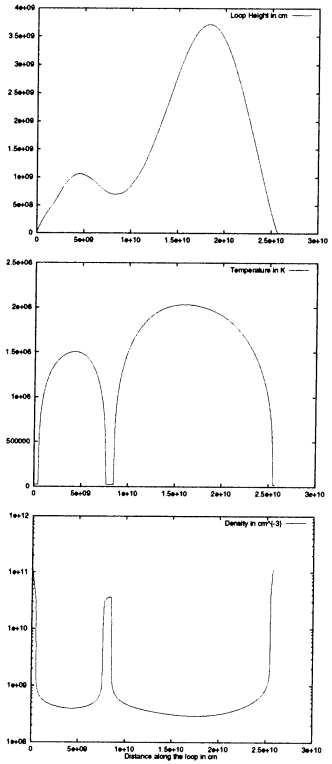

Temperature in K [1]

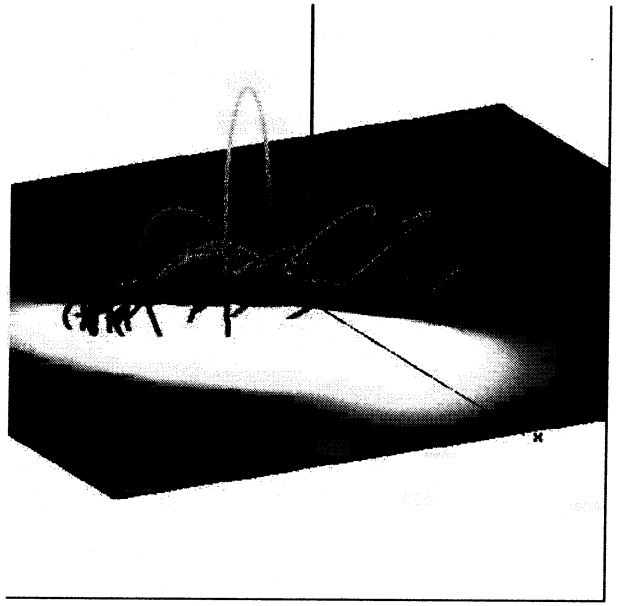

20000 2.7e6

Temperature in K [2]

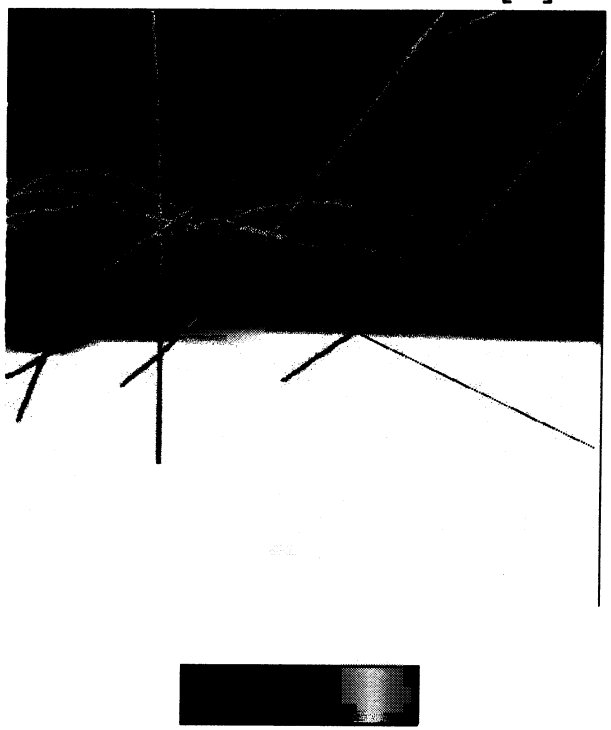

20000 2.7e6

Temperature in K [3]

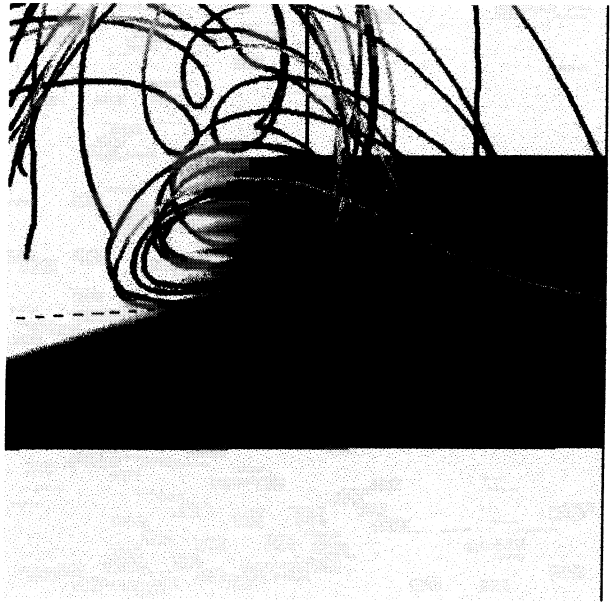

20000 2.7e6

Log Density in cm^{-3} [1]

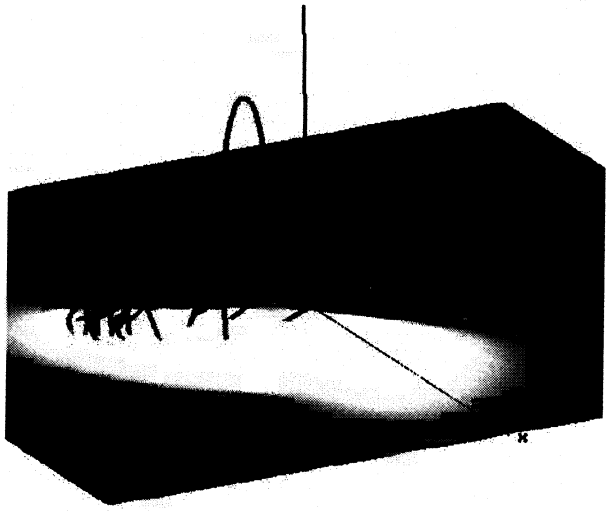

8.4 11.3

Log Density in cm^{-3} [2]

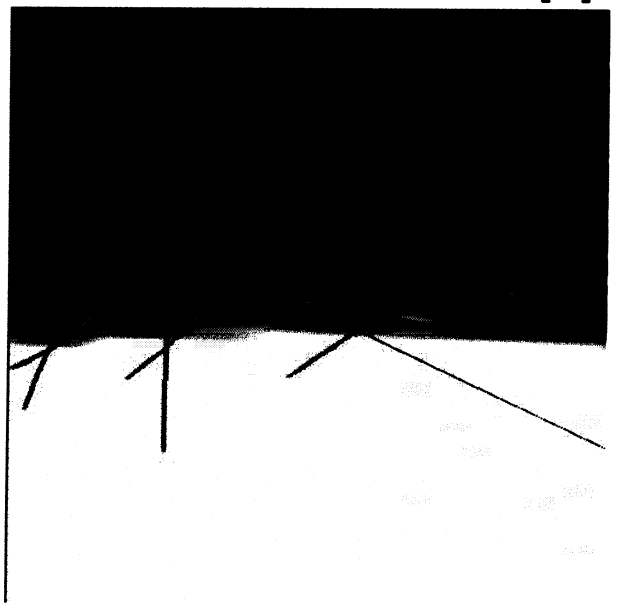

8.4 11.3

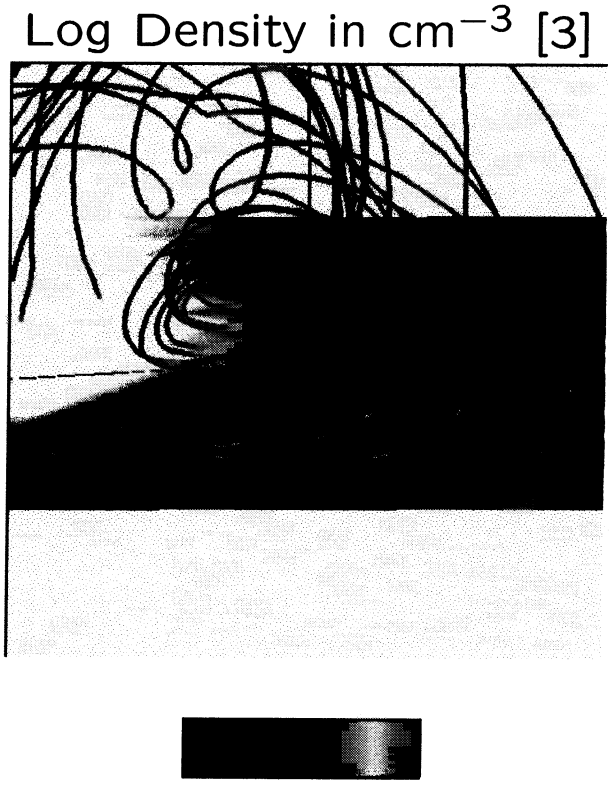

Conclusion

- We have shown how the process of emerging opposite polarity magnetic flux in a sheared realistic magnetic configuration can lead to the formation of a flux rope.

- Solutions of the hydrodynamic equations along the field lines of the flux rope show that the flux rope can support the dense and cold material, typical of a prominence.

- In the future we plan to do a self-consistent 3D MHD simulation with a more sophisticated model, which will incorporate coronal heating, thermal conduction and radiation losses.

REPORT DOCUMENTATION PAGE

Form Approved
OMB No. 0704-0188

1. AGENCY USE ONLY (Leave Blank)	2. REPORT DATE	3. REPORT TYPE AND DATES COVERED
	March 22, 2000	2nd Quarter 1st Year Progress Report (11/16/99 - 2/15/00)

4. TITLE AND SUBTITLE
"The Structure and Dynamics of the Solar Corona and Inner Heliosphere"
2nd Quarter 1st Year Progress Report

5. FUNDING NUMBERS
NAS5-99188

6. AUTHORS
Zoran Mikic

7. PERFORMING ORGANIZATION NAME(S) AND ADDRESS(ES)

Science Applications International Corporation
10260 Campus Point Drive MSW2M
San Diego, CA 92121-1578

8. PERFORMAING ORGANIZATION REPORT NUMBER
SAIC-00/8007:APPAT-241

9. SPONSORING/MONITORING AGENCY NAME(S) AND ADDRESS(ES)

NASA Headquarters Operation Office
Goddard Space Flight Center
Greenbelt, MD 20771

10. SPONSORING/MONITORING AGENCY REPORT NUMBER

11. SUPPLEMENTARY NOTES

12a. DISTRIBUTION/AVAILABILITY STATEMENT

12b. DISTRIBUTION CODE

13. ABSTRACT *(Maximum 200 words)*

This report details progress during the second quarter of the first year of our Sun-Earth Connections Theory Program Contract.

14. SUBJECT TERMS
Solar Corona, Coronal Magnetic Field, Heliosphere, Magnetohydrodynamics

15. NUMBER OF PAGES
24

16. PRICE CODE

17. SECURITY CLASSIFICATION OF REPORT	18. SECURITY CLASSIFICATION OF THIS PAGE	19. SECURITY CLASSIFICATION OF ABSTRACT	20. LIMITATION OF ABSTRACT
UNCLASSIFIED	UNCLASSIFIED	UNCLASSIFIED	UL